Article

"Attacking—Attacking" Anti-biofouling Strategy Enabled by Cellulose Nanocrystals—Silver Materials

Victor T. Noronha, Jennifer C. Jackson, Camilla H. M. Camargos, Amauri J. Paula, Camila A. Rezende, and Andreia F. Faria*

Read Online

ACCESS | Metrics & More | Article Recommendations | Supporting Information

ABSTRACT: The development of high-performance anti-biofouling surfaces is paramount for controlling bacterial attachment and biofilm growth in biomedical devices, food packing, and filtration membranes. Cellulose nanocrystals (CNCs), a carbon-nanotube-like nanomaterial, have emerged as renewable and sustainable antimicrobial agents. However, CNCs inactivate bacteria under contact-mediated mechanisms, limiting its antimicrobial property mostly to the attached bacteria. This study describes the combination of CNCs with silver nanoparticles (CNC/Ag) as a strategy to increase their toxicity and anti-biofouling performance. CNC/Ag-coated surfaces inactivated over 99% of the attached *Escherichia coli* and *Bacillus subtilis* cells compared to 66.9 and 32.9% reduction shown by the pristine CNC, respectively. CNC/Ag was also very toxic to planktonic cells, displaying minimal inhibitory of 25 and 100 μg/mL against *B. subtilis* and *E. coli*, respectively. CNC/Ag seems to inactivate bacteria through an "attacking—attacking" mechanism where CNCs and silver nanoparticles play different roles. CNCs can kill bacteria by piercing the cell membrane. This physical membrane stress-mediated mechanism is demonstrated as lipid vesicles release their encapsulated dye upon contact with CNCs. Once the cell membrane is punctured, silver ions can enter the cell passively and compromise the integrity of DNA and other organelles. Inside the cells, Ag⁺ may damage the cell membrane by selectively interacting with sulfur and nitrogen groups of enzymes and proteins or by harming DNA via accumulation of reactive oxygen species. Therefore, CNC/Ag toxicity seems to combine the puncturing effect of the needle-like CNC and the silver's ability to impair the cell membrane and DNA functionalities.

KEYWORDS: cellulose nanocrystals, antimicrobial nanomaterials, antimicrobial coatings, biofouling control, silver nanoparticles, cellulose nanocrystals-silver hybrid material, oxidative and membrane-mediated stress
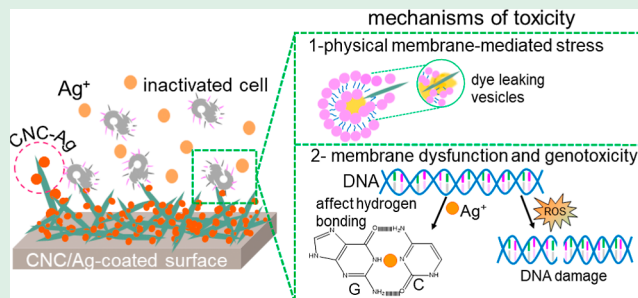
INTRODUCTION

Biofilms are ubiquitous and can form in various environments to protect microorganisms that adhere to surfaces. Biofouling has been a subject of great concern as attached cells are difficult to inactivate and can cause the corrosion of metal surfaces,[1] decline in membrane performance,[2−4] food spoilage,[5,6] spread of illnesses,[7] and damage to medical implants.[8,9] Preventing bacteria from forming biofilms over surfaces can reduce the economic costs from decreased equipment efficiency and human health impacts.

Intervention through antimicrobial coatings has been gaining research interest to reduce the impacts of biofilms.[10,11] Antimicrobial coatings generally mitigate biofouling either by inactivating the attached microorganisms or by preventing surface adhesion altogether. Carbon-based nanomaterials such as carbon nanotubes and oxide nanosheets have been widely used as antimicrobial coatings that function by deactivating microbes.[12−18] In contrast, polymer brushes such as zwitterionic polymers have been effectively applied for preventing microbial adsorption and organic fouling.[19−21] However, these materials

have the drawback of labor-intensive and time-consuming synthesis processes, limiting their application.

The foremost priority for developing antimicrobial surfaces should be applying sustainable materials produced on an industrial scale from waste or renewable source materials without using toxic and persistent chemicals. Cellulose nanocrystals (CNCs) are green and relatively inexpensive materials with promising antimicrobial properties. CNCs demonstrate antimicrobial activity comparable to other carbon-based nanomaterials[22] because of their great specific surface area and needle-like morphology.[22−24] Despite their excellent toxicity to bacteria,[22,23,25] CNCs inactivate cells under contact-mediated

mechanisms, limiting their ability to resist biofouling by killing planktonic cells in suspension.

Hybridization of CNCs with toxic metallic silver nanoparticles (AgNPs) is an advantageous strategy to improve the antimicrobial properties of CNCs and broaden their ability to inactivate bacteria in suspension and also those attached to surfaces.[26,27] This is especially advantageous for inactivating planktonic bacteria cells in aqueous media, where CNCs present limited toxicity.[22,23] AgNPs are easily synthesized, although their susceptibility to aggregation has a deleterious effect on their antimicrobial property. CNCs provide a large area for nucleation of silver, which favors the anchoring of nanoparticles while preventing agglomeration.[28,29] In addition, the synthesis process does not demand stabilizing agents, which are often non-biodegradable polymers or chemicals that are costly or toxic to humans and the environment. Capping agents can also affect the size distribution and morphology of the nanoparticles. The CNC surface contains many native hydroxyl and carboxyl functional groups, which work as anchoring sites for the deposition of AgNPs.[28] The association between AgNPs and CNCs can also improve CNC's toxicity, broadening its application as anti-biofouling agents. Another advantage of CNC/Ag is the residual toxicity of CNCs. After depleting the AgNPs, the remaining non-leachable and antimicrobial CNC can still impart toxicity to the surface.

In this study, we combine CNCs with AgNPs to fabricate hybrid materials that can inactivate cells through an "attacking–attacking" strategy, where both AgNPs and CNCs participate in the mechanism of toxicity. Attacking–attacking and attacking-defensive anti-biofouling strategies have been previously reported in the literature,[30−32] although not for CNC-based materials. CNCs were produced through hydrothermal treatment and subsequent (2,2,6,6-tetramethylpiperidin-1-yl)oxyl (TEMPO)-mediated oxidation of elephant grass (*Pennisetum purpureum*) biomass. AgNPs were anchored on CNCs using an *in situ* reaction with sodium borohydride, and the CNC/Ag was characterized using UV−visible light spectroscopy and transmission electron microscopy (TEM). We used vacuum filtration to deposit CNCs and CNC/Ag on the surface of polymeric filters and tested their anti-biofouling property against attached bacteria cells of *Escherichia coli* (Gram-negative) and *Bacillus subtilis* (Gram-positive). CNC and CNC/Ag coatings directly contact the bacteria cells, maximizing the anti-biofouling activity compared to the approaches that embed and entrap CNCs and CNC/Ag into polymeric matrices.[33,34] We also investigated the toxicity of CNCs and CNC/Ag against planktonic cells of the same bacteria described above. We performed encapsulated lipid vesicle assays to assess the ability of CNC/Ag to puncture bacteria cells. Also, glutathione (GHS) and H₂DCFA assays investigated the involvement of oxidative stress in the mechanism of toxicity of CNC/Ag, making this the first study to thoroughly assess the antimicrobial properties and mechanisms of action for CNC/Ag hybrid nanomaterials.

■ EXPERIMENTAL SECTION

Preparation and Characterization of CNCs−Silver (CNC/Ag) Hybrid Nanomaterials. CNCs in aqueous dispersion were obtained from elephant grass leaves using a previously reported protocol based on TEMPO-mediated oxidation and subsequent sonication of cellulose-rich fibers.[35] Afterward, CNC/Ag materials were produced using a methodology adapted from previous studies.[36,37] Briefly, 20 mL of a 1000 μg/mL CNC dispersion was prepared by resuspending an aliquot of the stock solution into DI water through bath sonication. In sequence, we added 2 mL of a 10 mM aqueous AgNO₃ solution into the

CNC dispersion. After stirring for 1 h, 2 mL of a 10 mM aqueous NaBH₄ solution was added into the dispersion, which was stirred for another hour. The CNC/Ag dispersion was collected in a dialysis membrane (3.5 KDa molecular weight cut off, Spectra/Por membrane, Spectrum Laboratories, USA) and dialyzed against deionized (DI) water for 2 h. After dialysis, the resulting CNC/Ag dispersion was collected and used in further assays. Based on the initial quantity of the precursors utilized, CNC and Ag concentrations were estimated at 833 μg/mL and 0.833 μM, respectively. TEM was used to investigate the morphology of CNC/Ag. 10 μL of a CNC/Ag suspension (∼10 μg/mL) was deposited in a 400-mesh carbon-coated Formvar nickel grid (Ted Pella, Redding, CA). The CNC/Ag-containing grid was coated with 10 μL of 0.5% uranyl acetate solution for 30 s and air-dried. CNC/Ag was examined with FEI Tecnai G2 Spirit Twin TEM (FEI Corp., Hillsboro, OR, USA) equipped with a UltraScan camera and Digital Micrograph software (Gatan Inc., Pleasanton, CA, USA). The average diameter of the AgNPs was measured considering 134 particles analyzed using the software ImageJ.

The chemical characteristics of the CNC and CNC/Ag hybrid nanomaterial were analyzed using X-ray photoelectron spectroscopy (XPS) as described in our previous publication.[38] Attenuated total reflection Fourier-transformed infrared spectroscopy (ATR-FTIR) spectra of freeze-dried CNC and CNC/Ag samples were acquired with a resolution of 4 cm⁻¹ and 128 scans using a Cary 630 FTIR spectrometer (Agilent Technologies, Santa Clara, CA, USA).

The concentration of Ag⁺ ions released by CNC/Ag was measured by adapting a previously reported protocol.[34] First, 15 mL of an aqueous dispersion of 1500 μg/mL CNC/Ag (in triplicate) was dialyzed against 100 mL of DI water for up to 24 h. The volume of Ag⁺ solution (100 mL) was collected immediately at the beginning of the dialysis process and every 1 h for 6 h and then after 12 and 24 h and exchanged with clean DI water. The collected solutions were acidified with 0.2% (w/w) HNO₃, and the concentration of released Ag was measured using atomic absorption spectrometry in an atomizer AA600 graphite furnace (GFAAS, PerkinElmer, Waltham, MA, USA). The Supporting Information describes the details of CNC and CNC/Ag characterization via X-ray diffraction (XRD), thermogravimetric analysis (TGA), zeta potential, and dynamic light scattering (DLS).

Anti-biofouling Activity of CNCs and CNC/Ag-Coated Surfaces. Aqueous dispersions containing 500 μg/mL of either CNC/Ag or CNCs in DI water were prepared and filtered through a 0.22 μm polyvinylidene difluoride (PVDF) filter in a manifold, resulting in CNCs and CNC/Ag-coated filters. Pristine PVDF filters without a deposited nanomaterial were used as control samples. *E. coli* (American Type Culture Collection ATCC 8739) and *B. subtilis* (ATCC 6633) were cultivated in LB at 37 and 30 °C, respectively, in an incubator. After overnight growth, 1 mL of each bacterial suspension was mixed with 24 mL of fresh LB broth (1:25) and kept under agitation until the suspension could reach around 1.0 of optical density at 600 nm, indicating exponential growth (∼2 h). The resulting suspension was then centrifuged, and the recovered bacterial cells were washed three times with sterile 0.9% NaCl solution. The suspended cells were then 10-fold diluted in a sterile saline solution to obtain a 10⁸ CFU/mL (colony-forming units per mL) bacterial suspension. 3 mL of the bacterial suspension was placed in each manifold well and incubated for 3 h. Then, the bacterial suspension was gently removed, and the surface of the filters was rinsed with a sterile saline solution to remove the non-attached bacteria. The coated filter was then transferred to a 50 mL centrifuge tube filled with 10 mL of saline solution and subjected to bath sonication for 15 min in order to detach any adhered bacteria from the CNC and CNC/Ag-coated surfaces. The concentration of cells in each suspension was quantified via plate counting.[22] All tests for antimicrobial activity were carried out in triplicate.

Morphological Characterization of the Attached Bacteria Cells. Scanning electron microscopy (SEM) was performed to assess the morphological characteristics of the cells attached to the coated surfaces as carefully described in our previous study.[22]

Antibacterial Properties of CNCs and CNC/Ag to Planktonic Bacteria Cells. Minimal inhibitory concentration (MIC) and minimal bactericidal concentration (MBC) of the nanomaterials were
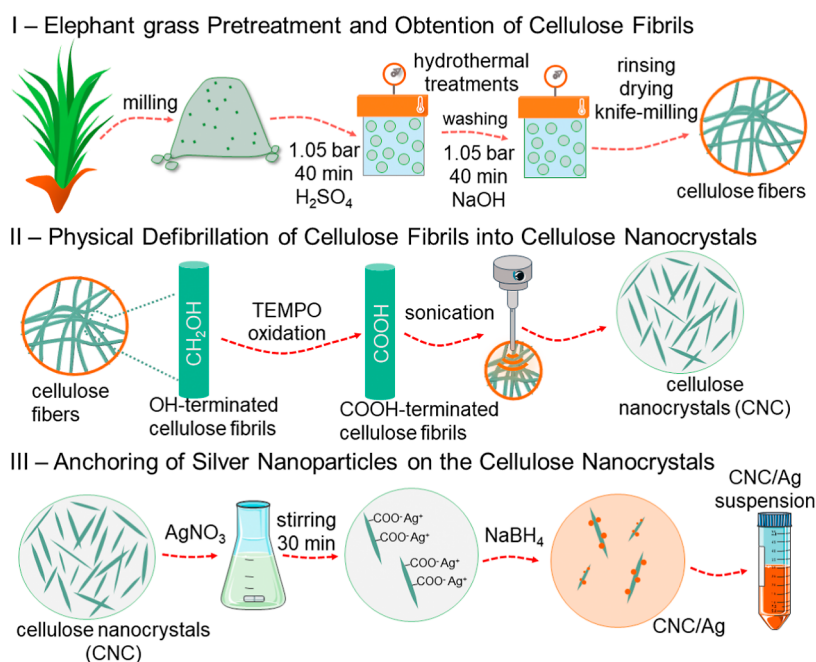
Figure 1. Illustration of the complete CNC/Ag synthesis process. (I) Elephant grass leaves are milled and subjected to a two-step hydrothermal pretreatment with dilute sulfuric acid and sodium hydroxide solutions. This process culminates in the extraction of cellulose-rich fibers. (II) The cellulose-rich fibers undergo an oxidation process with TEMPO, NaBr, and NaClO. The resulting carboxyl-rich fibers are mechanically defibrillated through probe ultrasonication for 60 min to obtain the CNCs. (III) Finally, AgNO$_3$ and NaBH$_4$ are sequentially added to the CNC dispersion for an *in situ* anchoring AgNPs onto CNCs.

determined through the microdilution method, using a protocol based on CLSI (Clinical & Laboratory Standards Institute) guidelines.[18,39] Briefly, *E. coli* or *B. subtilis* cells cultivated in lysogeny broth (LB) agar plates were placed in 10 mL of LB and incubated overnight at their optimum temperature growth (37 °C for *E. coli* and 30 °C for *B. subtilis*). After growth, an aliquot of each suspension was resuspended in a fresh saline solution (0.9% NaCl) to reach an OD$_{600}$ (optical density at 600 nm) between 0.08 and 0.12. After that, 200 μL of each bacterial suspension was individually transferred to 30 mL of fresh LB broth, resulting in an estimated bacterial concentration of 10^6 CFU/mL. 1 mL of each bacterial suspension was mixed with 1 mL of each nanomaterial dispersion (CNC or CNC/Ag) in reaction vials to reach final concentrations of 0, 10, 25, 50, 75, 100, 150, 200, 250, and 300 μg/mL. The vials containing the cells and the nanomaterials were vortexed, and 200 μL of each sample was pipetted into a 96-well plate. Each concentration of the nanomaterial (CNC or CNC/Ag) was pipetted in six individual wells. The plates were incubated for 18−24 h at the optimum temperature for each bacteria strain. Following incubation, the optical density in each well was quantified using a microplate reader (SpectraMax M5 Multi-Mode, Molecular Devices, Sunnyvale—CA, USA). The optical density of the wells at the initial time of the incubation was used as a control. Absorbance values are expressed as final readings subtracted from the initial measurements. MIC is the lowest concentration of the nanomaterial able to inhibit bacterial growth after overnight incubation. Given that the optical absorbance of a bacterial suspension relates to bacteria growth, unchanged optical absorbances after 18 h incubation indicate no detectable bacterial growth.

For MBC determination, 20 μL of the control sample (without nanomaterials) was added to 20 mL of saline solution. After homogenization, 100 μL of the resulting suspension was cultivated on LB plates in triplicate. 20 μL aliquots were withdrawn from the wells containing the MIC and from the two wells next to the highest concentration of the nanomaterial (CNC or CNC/Ag) and subsequently spread on LB agar plates to determine the number of CFU/mL. The MBC value is the concentration able to reduce at least 99.9% of the number of viable colonies when compared to the starting inoculum. The MBC/MIC ratio can be used to categorize the

antibacterial activity, with a ratio between 1 and 2 corresponding to bactericidal activity, and a value higher than 2 that corresponds to a bacteriostatic effect.[18]

Evaluating the Time-Dependent Toxicity of CNCs and CNC/ Ag to Planktonic Cells. To assess the antibacterial activity of the nanomaterial over time, we carried out experiments using a CLSI-based protocol.[18,39,40] CNC/Ag was used at their MIC for each bacterial strain (25 μg/mL for *B. subtilis* and 100 μg/mL for *E. coli*). CNC dispersions with the same concentration as the CNC/Ag dispersions were used as comparative controls. An aliquot (varying from 200 to 1000 μL) from an overnight grown bacterial suspension in LB of each bacteria strain was transferred to a glass vial containing 5 mL of saline solution, adjusting the OD$_{600}$ to 0.08−0.12. A 200 μL aliquot of each of these suspensions was added to 30 mL of LB, resulting in ∼10^6 CFU/ mL. Reaction vials were prepared by mixing 1 mL of the resulting bacterial suspension and 1 mL of the nanomaterial dispersion, for a final concentration of 25 μg/mL (CNC and CNC/Ag × *B. subtilis*) or 100 μg/mL (CNC and CNC/Ag × *E. coli*). DI water (1 mL) was used for the control samples. The vials were incubated at room temperature and 60 rpm. A 100 μL aliquot of each vial was withdrawn at different incubation times (0, 1, 2, 3, 4.5, and 6 h) and serial diluted (1:10, 1:100, 1:1000, 1:10000) in saline solution. Five 20 μL drops from each dilution were plated on LB agar and incubated overnight at the respective optimum temperature for each bacteria strain. Bacterial concentration was then calculated after colony counting. The assays were performed in triplicate.

***In Vitro* Oxidation of GHS after Exposure to CNCs and CNC/ Ag.** The GSH assay has been consistently used to determine the nanomaterial ability to induce oxidative stress.[41] GHS is a natural antioxidant that protects the cells against oxidative stress.[42,43] Under the presence of oxidative species, GHS is oxidized to its disulfide form. The amount of oxidized GHS is directly related to the oxidative potential of the nanomaterial.[41] The non-oxidized GHS reacts with Ellman's reagent, producing a yellow compound (3-thio-6-nitro-benzoate, TNB) for which optical absorbance was quantified in a spectrophotometer (Hitachi U-2900, Japan). Details of this protocol can be found in our previous study.[22] The amount of TNB present is directly related to GSH oxidized and can be then calculated using an

extinction coefficient of 14150 M^{-1} cm^{-1} and a pathlength of 1 cm. A solution without nanomaterial was used as a negative control, and a H_2O_2 solution (10 mM) was used as a positive control. Residual amounts of GHS in each sample were obtained, and the results were expressed as loss of GSH (%) compared to the control sample (without nanomaterials).

Quantification of Intracellular Reactive Oxygen Species Promoted by Exposure to CNC/Ag. Reactive oxygen species (ROS) inside the bacteria cells generated after exposure to CNC/Ag was evaluated using H_2DCFDA as a probe, as previous described elsewhere.[22,44] First, 1.9 mL of a 10^8 CFU/mL *E. coli* suspended in 0.1% peptone water was mixed with 100 μg/mL CNC/Ag dispersion. The vials were incubated for 3 h at 60 rpm and room temperature. A volume of 40 μL of H_2DCFDA (10 mM, dissolved in ethanol) was added to 2 mL of the bacteria-CNC/Ag suspension, for a final H_2DCFA concentration of 0.2 mM. Vials were covered with aluminum foil and kept away from the light for 15 min. Another volume of 200 μL was transferred to a 96-well plate for fluorescence measurements. Intracellular esterases hydrolyze H_2DCFDA into H_2DCF (2′,7′-dichlorodihydrofluorescein), a nonfluorescent compound that remains inside the cells. Under the presence of ROS and intracellular peroxidases, H_2DCF is transformed into a highly fluorescent compound named DCF (2′,7′-dichlorofluorescein). The fluorescence signal correlates to the presence of ROS inside the bacteria cells. The fluorescence signal was quantified in a Cytation 5 microplate reader (Biotek Instruments, Vermont, USA) using 493 and 520 nm as excitation and emission wavelengths, respectively. Menadione (100 μM), an oxidant agent known for inducing ROS generation,[45] was used as a positive control. The fluorescence intensity was normalized to the control samples without nanomaterial.

Preparation of Dye-Containing Lipid Vesicles and Dye-Leaking Assay. Dye-containing lipid vesicles were used to analyze the ability of CNCs and CNC/Ag to disrupt lipid bilayers, as performed in previous studies.[46,47] Details of the protocol used to prepare the dye-containing vesicles is found in our previous study.[22]

To perform the dye-leaking assay, 822 μL of the prepared vesicle suspension was mixed with each nanomaterial, yielding a final CNC and CNC/Ag concentration of 200 μg/mL in 1.5 mL. The mixtures were kept under rocking agitation for 3 h at room temperature. Afterward, the suspensions were vortexed for 10 s, and the resulting mixtures were centrifuged at 15,000 rcf for 15 min. The absorbance of the supernatant at 500 nm was measured in a Genesys 30 spectrophotometer (Thermofisher Scientific, Waltham, MA, USA). For the negative control, DI water was used instead of the nanomaterial dispersion. Each treatment was prepared and analyzed in triplicate. To determine the maximum absorbance intensity (Abs_{max}), a suspension of vesicles was mixed with 0.1 g/mL sodium lauryl sulfate (SLS), which promotes the releasing of acridine orange into the solution. The average absorbance intensity from each treatment was divided by the average maximum absorbance (Abs_{max}) obtained from SLS-treated solution, and the results are shown as normalized values.[48]

■ RESULTS AND DISCUSSION

Characteristics of CNCs and CNC/Ag. TEMPO-oxidized CNCs were used as a platform to anchor AgNPs. The existence of sodium carboxylate and hydroxyl functional groups on the CNC surface favors the ion exchange from Na^+ to Ag^+ ions upon the addition of $AgNO_3$.[49,50] The attached Ag^+ ions were reduced in situ by $NaBH_4$ to form AgNPs immobilized on the CNC surface.[36,49] The complete synthesis process is depicted in Figure 1.

Figure 2A shows photographs of both pristine CNC and CNC/Ag dispersions. The pristine CNC dispersion displays a transparent whitish color. In contrast, the CNC/Ag dispersion is brownish, a distinctive visual characteristic that indicates the presence of AgNPs in the system. The absorption band around 420 nm in the UV−vis spectra of the CNC/Ag sample corresponds to the surface plasmon resonance (SPR) effect
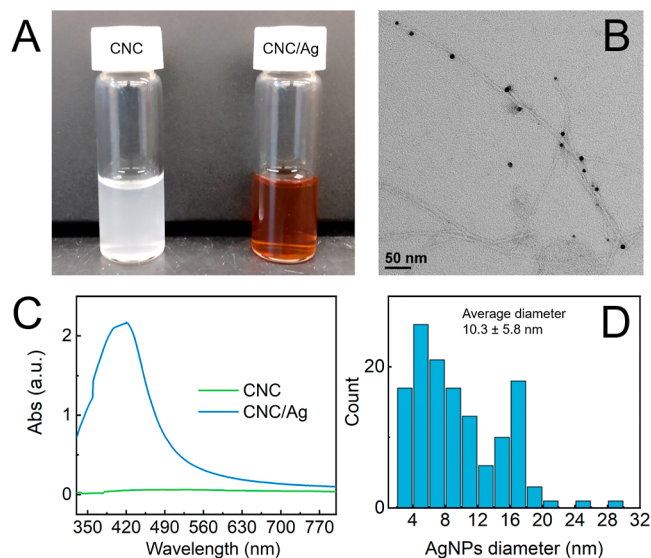
Figure 2. (A) Photos of CNC and CNC/Ag dispersions, (B) TEM micrograph of CNC/Ag particles, (C) UV−vis absorption spectra of pristine CNC and CNC/Ag dispersions, and (D) histogram showing the size distribution of AgNPs anchored onto CNCs. AgNPs anchored to CNCs show an average diameter of 10.3 nm.

promoted by AgNPs.[51] Its appearance suggests the anchoring of the metallic AgNPs on the CNC surface (Figure 2C). XRD profiles of both CNCs and CNC/Ag show typical cellulose I diffraction peaks at around 15.6, 22.6, and 34.4°, corresponding to the cellulose planes 101, 002, and 040, respectively.[52] On the other hand, the peak at 38.7° in the XRD pattern of CNC/Ag corresponds to the 111 plane of the AgNPs (Figure S1).[53] TGA was conducted to estimate the relative amount of silver in the CNC/Ag material (Figure S2). After thermal decomposition, the remaining mass for the CNC sample was 1.18%, while the ash content in the CNC/Ag sample was 12.54% of its initial weight. This result indicates that the amount of Ag anchored in CNCs was around 11 wt %, which is congruence with previous studies.[54,55]

The morphological properties of CNCs and the nucleation of AgNPs on CNC/Ag were confirmed through TEM (Figures S3 and 2B). TEM images show dark particles attributed to the spherical AgNPs distributed on the CNC surface (Figure 2B). The electrostatic interactions between the positively charged Ag^+ ions and the anionic oxygen-containing functional groups on CNCs lead us to postulate that AgNPs are homogeneously and tightly anchored on the CNC backbone.[28,36,49] As previously discussed elsewhere,[28] the strong interactions between both constituents facilitate silver nucleation, preventing the growth of large and polydisperse AgNPs. The AgNPs decorating the CNC surface show a narrow diameter distribution and an average diameter of ∼10.3 ± 5.8 nm (Figure 2D). AgNPs immobilized onto TEMPO-oxidized bacterial cellulose nanofibers have demonstrated an average diameter of 10−20 nm,[49] while AgNPs immobilized on porous cellulose fibers have shown a size of approximately 7.9 ± 2.4 nm.[28] In addition, AgNPs anchored to the surface of acid-hydrolyzed or TEMPO-oxidized CNC have shown an average size varying from 25 nm[56] to 9.7 ± 3.6 nm,[36] respectively, which corroborates with the particle size described herein.

As shown by the XPS data, the Ag 3d doublet peak near 370 eV confirms the presence of AgNPs in the CNC/Ag nanomaterial (Figure S4). The higher resolution spectrum in Figure S4B

shows that the Ag 3d doublet consists of two conjugated peaks located at 369.9 eV, attributed to Ag 3d$_{5/2}$, and 375.9 eV, assigned to Ag 3d$_{3/2}$. The energy of 6.0 eV separating the conjugated peaks is assigned to the presence of zero-valent silver,[57,58] indicating the existence of metallic AgNPs in the CNC/Ag hybrid nanomaterial. ATR-FTIR analyses confirmed that the characteristic chemical structure of cellulose was still present in the CNC/Ag hybrid nanomaterial (Figure S5). The decrease in the intensity for the absorption bands attributed to the stretching vibration of carboxyl[38] and hydroxyl groups at 1600 and 3330 cm^{-1}, respectively, can be related to the electrostatic interactions between AgNPs and the oxygen-containing functional groups on the CNC.[59]

The release of Ag$^+$ ions from CNC/Ag into water was evaluated using atomic absorption spectrometry. As shown in Figure S6, in the first hour of leaching, the concentration of Ag$^+$ ions increased from about 0.1 to 5.3 μg/L per mg of CNC/Ag. After a steady release of ~4 μg/L within the first 5 h, the concentration of Ag$^+$ ions increased to 8.7 μg/L/mg of CNC/Ag after 24 h. The absolute amount of Ag$^+$ released per 1000 μg of CNC/Ag after 24 h was approximately 0.9 μg, thus resulting in a prolonged antibacterial performance of the hybrid nanomaterial.[34] Ag$^+$ ions at a minimum concentration of 0.1 μg/L render a high antimicrobial efficacy, as these ions are capable to interact strongly with electron donor groups (S, O, and N groups) in biological molecules.[60]

To evaluate the effect of silver decoration on the colloidal stability of CNC/Ag, we conducted zeta potential measurements of CNC and CNC/Ag dispersions in DI water (Figure S7). As indicated by the data in Figure S7, the presence of AgNPs has not affected the zeta potential of CNCs. The zeta potential for the CNC remained unchanged before (−54.6 ± 13.9 mV) and after (−54.0 ± 6.81 mV) functionalization with the AgNPs. Since the zeta potential values for CNCs and its derivative nanomaterial CNC/Ag are very similar, we would expect them to present similar colloidal stability at the conditions investigated in this study.

CNC and CNC/Ag-Coated Surfaces Inactivate Attached Bacteria Cells. We evaluated the interaction between bacterial cells and CNC and CNC/Ag-coated surfaces through a contact-mediated assay (Figure 3). Suspensions of each *E. coli* and *B. subtilis* interacted with the coated surfaces produced by the deposition of the nanomaterials onto a PDVF filter.

As shown in Figure 3, CNC-coated surfaces were effective against both *E. coli*- and *B. subtilis*-attached cells. Surfaces coated with pristine CNCs presented 66.9 and 32.9% inactivation rates for attached *E. coli* and *B. subtilis* cells, respectively. We postulate that under direct contact with the CNC-coated surface, the thicker peptidoglycan layer in the cell wall of *B. subtilis* acts as a physical barrier, hindering the piercing effect of the CNC. Indeed, a previous investigation shows that CNCs inactivate bacteria by puncturing and disturbing the physical integrity of the cell membrane.[22] Therefore, the anti-biofouling activity observed for CNC-coated surfaces is attributed to a contact-dependent mechanism triggered by the bacteria attachment to the CNC-coated surface.

Although CNC-coated surfaces display significant antimicrobial properties, their toxicity was enhanced through functionalization with antimicrobial AgNPs (CNC/Ag) (Figure 3). CNC/Ag-coated surfaces showed improved anti-biofouling properties compared to CNCs or uncoated surfaces. The number of viable adhered *E. coli* and *B. subtilis* cells was reduced by approximately 99% under contact with the CNC/Ag-coated
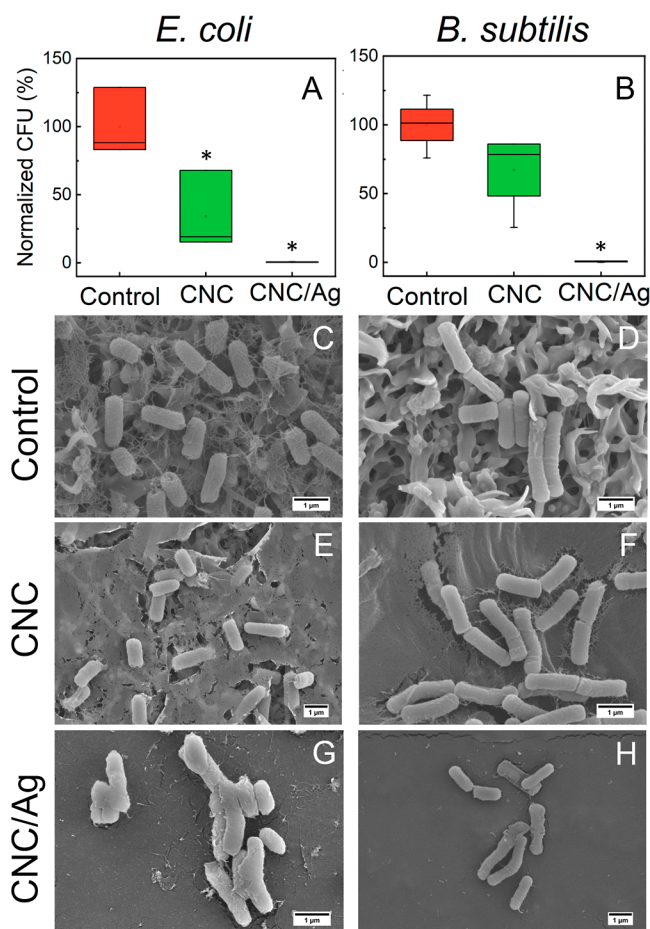

Figure 3. Bacterial viability of adhered *E. coli* (A) and *B. subtilis* (B) cells after 3 h of exposure to CNC and CNC/Ag-coated surfaces. Plate counting was carried out to determine the cellular viability. The number of viable cells is shown as a percentage value normalized to the pristine PVDF membrane (uncoated surface). Asterisks indicate a statistical difference from the control sample (α = 0.05). SEM images showing *E. coli* and *B. subtilis* cells after exposure to pristine PDVF filters (C,D, respectively), CNC-coated filters (E,F), and CNC/Ag-coated filters (G,H). Scale bars: 1 μm.

filters, a significantly increased toxicity compared to the CNC-based coatings. Similar anti-biofouling properties were observed for CNC/Ag-coated surfaces against Gram-positive and Gram-negative bacteria, indicating that the CNC/Ag coatings can effectively inactivate both model bacteria.

Previous works report on the application of CNC/Ag particles as antimicrobial agents. For instance, Xu et al. have embedded CNC/Ag into polymeric thin films at different concentrations. The thin films containing CNC−Ag could inactivate 99.4% of attached *E. coli* cells after 3 h exposure.[34] In another study, polyvinyl alcohol membranes embedded with CNC/AgNPs have shown strong antibacterial activity against *E. coli* and *S. aureus*. After 24 h of exposure to the modified membranes, attached *E. coli* and *S. aureus* cells have been inactivated at rates of 96.9 and 88.2%, respectively.[37] However, the approach described herein is more advantageous compared to the studies described above. Instead of embedding CNCs or CNC/Ag in the polymeric matrix, the coated surfaces enable direct contact of CNC/Ag with the bacteria. Embedding approaches lead to CNC/Ag entrapment within the bulk structure of the polymer, preventing direct contact between bacteria and the nanomateri-
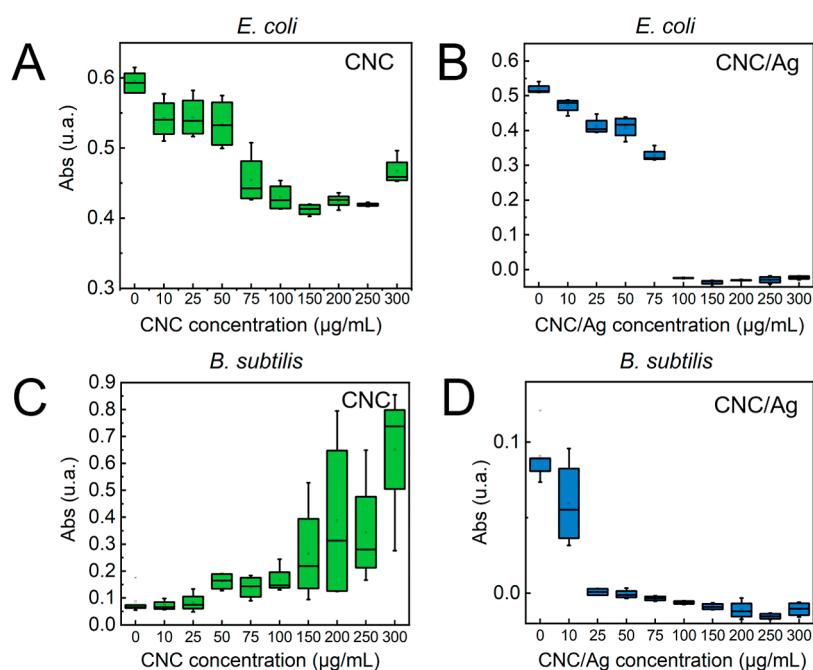
Figure 4. Absorbance (OD_{600}) of *E. coli* suspensions exposed to (A) pristine CNCs and (B) CNC/Ag. Absorbance of *B. subtilis* cell suspension contacted with (C) pristine CNCs and (D) CNC/Ag. The antimicrobial assays were performed in 96-well microplates, and the optical absorbance was quantified after 18 h of incubation. Bacterial suspensions were exposed to increasing concentrations (0 to 300 μg/mL) of CNCs (A,C) and CNC/Ag (B,D). Absorbance readings for the bacteria suspensions were subtracted from their negative controls (without bacteria cells). Light absorption on microwell suspensions can be directly related to bacterial growth. Standard deviations of four replicates are represented by the error bars.

al. As CNC/Ag is embedded in the polymeric matrix, the composite material cannot profit from the contact-mediated toxicity of CNCs since it is not available at the surface to contact the cells directly. In the end, the antimicrobial properties of CNC/Ag reflect the toxicity of the AgNPs with little or no involvement of CNCs. Therefore, the strategy of depositing CNCs and CNC/Ag on the surface of polymeric materials can maximize their contact with bacteria cells, leading to improved anti-biofouling properties.[12,22,61] Surface coating is attractive for CNC-based nanomaterials because of their ability to inactivate bacteria through a contact-dependent route.[22]

The morphological characteristics of bacteria cells adhered to the CNC and CNC/Ag-coated surfaces were evaluated by SEM analysis (Figure 3). Both *E. coli* and *B. subtilis* cells attached to the PVDF filters presented higher levels of cell integrity, as observed in Figure 3C,D. In contrast, *E. coli* and *B. subtilis* cells adhered to CNC/Ag-coated surfaces showed a flatten and shrunken morphology, as seen in Figure 3G,H, respectively. Loss in cell integrity and morphology is due to the interaction between the bacteria cells and the sharp edges of the CNC. Previous studies proposed that the needle-like shaped CNC can cause contact-mediated damages to the bacteria cell through the interaction with its sharp edges.[22,62] Additionally, the presence of AgNPs on CNC/Ag-coated samples further enhanced the antimicrobial effects, resulting in a combined "attack–attack" toxic effect on bacteria. The AgNPs in CNC/Ag dissolve into Ag^+ ions with an affinity for several vital biomolecules and organelles, such as DNA, peptides, enzymes, and cofactors. By binding to these bio-structures, the Ag^+ ions disrupt the cell metabolism, culminating in cellular death.[22,62,63] Therefore, the loss of morphological characteristics observed for the cells exposed to CNC/Ag is likely a combination of physical stress caused by the sharp CNC and chemical-mediated stress created

by the action of silver ions on the cell membrane proteins and DNA.

Confocal microscopy has also been performed to evaluate the biofilm formation over the surfaces of pristine and PVDF filters coated with CNCs and CNC/Ag. The average biovolumes of *E. coli* dead cells on pristine, CNC-coated, and CNC/Ag-coated filters were 0.00027, 0.00929, and 0.03958 μm^3/μm^2, respectively (Figure S8). These results indicate a significant increase in the density of dead cells (by a factor of 35 and 148, respectively) for filters coated with CNCs and CNC–Ag compared to the uncoated filter surface. For *B. subtilis*, similar results have been observed. The average biovolume for dead cells increased from 0.00013 to 0.00507 and 0.01122 μm^3/μm^2 for CNCs and CNC/Ag-coated filters, respectively (a factor of 39 and 87 compared to pristine PVDF control, respectively).

Despite the larger biovolume of dead cells, we can still observe a large number of live cells (green color) on the CNC and CNC/Ag-coated samples, as indicated in Figures S8A,B. Since the assay has been performed in static conditions, it is likely that the first layer of dead bacteria cells and their components/debris are shielding to some extent the toxicity of the CNC/Ag-coated surfaces and allowing bacterial growth. This effect could be minimized under non-static conditions, where water flow and better diffusion of oxygen could maximize the oxidation of the AgNPs anchored on the CNC/Ag, providing an improved release of Ag^+ ions into the solution and mobility of attached and non-attached bacteria cells.[64] More details on this assay can be found in the Supporting Information, page S5.

Antibacterial Activity of CNCs and CNC/Ag against Planktonic Bacteria Cells. To broaden the application of CNC/Ag as an anti-biofouling agent, we also tested the toxicity of CNC/Ag against planktonic cells. Figure 4 shows the toxicity of CNCs and CNC/Ag to *E. coli* and *B. subtilis*, Gram-negative and Gram-positive bacteria, respectively. At CNC concen-

trations of 75 μg/mL and above, we detect a reduction in *E. coli* growth. Despite that, we could not observe a complete inhibition of *E. coli* cells at any tested CNC concentrations. Since CNC could not inhibit bacterial growth at the tested concentrations, we could not estimate its MIC against *E. coli*. In contrast, CNC/Ag was very toxic to *E. coli* cells at all tested concentrations. At a MIC of 100 μg/mL, CNC/Ag inactivated 100% of the *E. coli* cells compared to the control. These findings indicate an improved antimicrobial effect for CNC/Ag compared to unmodified CNCs (Figure 4A,B).

As shown in Figure 4C, it seems that the presence of CNCs promoted *B. subtilis* growth, which is reflected by the rising absorbance values as the CNC concentration increased. We presume that CNCs promote sporulation of *B. subtilis* by creating a hostile environment for the bacteria cells. As *B. subtilis* sporulates, the spores form large aggregates (some visible to the naked eye, as shown in Figure S9), increasing the optical density of the bacterial suspension. This phenomenon becomes more pronounced as the CNC concentration increases. Production of spore-containing agglomerates is a well-documented behavior for *B. subtilis*.[65] Despite the CNC's lack of toxicity, CNC/Ag efficiently suppressed the *B. subtilis* growth starting at concentrations of approximately 25 μg/mL (Figure 4D). *E. coli* cells presented a much higher MIC than *B. subtilis* when exposed to CNC/Ag. *B. subtilis* displayed a 25 μg/mL MIC, four times lower than the MIC value of *E. coli* cells (100 μg/mL) after contacting CNC/Ag in suspension. These results indicate a higher susceptibility of *B. subtilis* to CNC/Ag under the tested conditions. Our results agree with a previous study showing MIC values of 125 μg/mL for *E. coli* and 15.6 μg/mL for *B. subtilis* treated with cellulose nanowhiskers modified with AgNPs.[66] Similar antimicrobial properties have been also reported for other Ag-based carbon nanomaterials, including organic framework (MOF)[67−69] and graphene oxide modified with AgNPs.[17−19,70]

During MBC assessment, no colony growth was observed on the LB agar plates for *E. coli* or *B. subtilis* incubated with CNC/Ag at concentrations equal or higher than the MIC. This phenomenon implies that MBC is equivalent to the MIC values for both bacteria strains (Table 1). The MBC/MIC ratios for *E.*

Table 1. MIC and MBC for CNC and CNC/Ag Tested against *E. coli* and *B. subtilis*

strain	MIC (μg/mL)		MBC (μg/mL)		MBC/MIC
	CNC	CNC/Ag	CNC	CNC/Ag	CNC/Ag
E. coli (ATCC 8739)		100		100	1
B. subtilis (ATCC 6633)		25		25	1

coli and *B. subtilis* were equal to 1, indicating a bactericidal effect for CNC/Ag in suspension. Similar MBC/MIC ratios have been found for the interaction of *E. coli* and *B. subtilis* with Ag-based hybrid materials in the literature.[66] MBC values were not obtained for pristine CNCs since we could not determine its MIC for either *E. coli* or *B. subtilis*.

It is worth pointing out that the presence of electrolytes can affect the colloidal stability of CNC/Ag dispersions and their toxicity in suspension. For rod-like sulfated CNCs, the reported critical coagulation concentration (CCC) of NaCl was 153 mM.[71] Changes in stability and dispersibility promoted by salt concentrations above the CCC should affect the antimicrobial performance of CNCs in suspension, since its mechanism of

action rely partially on the puncturing effect promoted by the sharp edges of well-dispersed nanocrystals. In this study, we use TEMPO-oxidized CNCs and the LB broth media contains 43 mM NaCl, as indicated by the manufacturer. TEMPO-oxidized CNCs possess larger number of anionic carboxyl containing functional groups and higher surface charge density than sulfated CNCs.[35] In addition, the NaCl concentration in the LB broth medium used in the antimicrobial assays is significantly lower than that required to modify the stability of CNCs in aqueous solutions.[71] Under such salinity, the colloidal stability of CNCs should remain unchanged.

To confirm the colloidal stability of CNC/Ag, we measured the hydrodynamic diameter of CNC/Ag dispersed in LB broth (environment of the antimicrobial assays) and DI water (final concentration of 300 μg/mL) using DLS over 6 h (Figure S10). Due to the non-spherical nature of CNCs, we expected that the Z-average value obtained through DLS would not necessarily match neither the length nor the width of the CNC/Ag particles. Rather, this value corresponds to the "apparent size" of an equivalent sphere with the same diffusion coefficient as the dispersed CNC/Ag. Despite the limitations, the DLS analysis can provide useful information regarding the emergence of agglomerates and aggregates in the solution.[72] As shown in Figure S10, the hydrodynamic size values remained steady during the analysis, with a slightly increasing tendency for CNC/Ag dispersed in LB broth compared to CNC/Ag dispersed in water. The average hydrodynamic diameter obtained for CNC/Ag dispersed in LB (599.6 ± 262.2 nm) may indicate the presence of weakly bounded particles, since this value is higher than the average length value for CNC/Ag suspended in DI water (143 ± 64.4 nm).

To evaluate the possible presence of severe agglomeration, we also monitored the colloidal stability of CNC/Ag using the characteristic SPR frequency (∼400 nm) of AgNPs under excitation at the UV−vis. For that, we performed UV−vis spectroscopy analyses of CNC/Ag suspended in LB broth over different time intervals (Figure S11). The absorbance spectra of CNC/Ag suspended in LB at 100 μg/mL were taken every hour up to 6 h and after 24 h. A complete description of the experimental protocol has been added to the Supporting Information on Page S4. We observed a decrease in intensity and broadening of the SPR band at ∼ 400 nm for CNC/Ag dispersed in LB, suggesting possible formation of weakly bonded particles.[73,74] The reduced intensity of SPR band alone could also indicate the dissolution of the AgNPs.[73] Despite the decrease in SPR intensity over time, we did not observe additional absorbance bands in wavelengths above 600 nm that would have be indicators of heavy agglomeration.[73,74] Therefore, although some particle−particle interaction may be occurring, severe signs of agglomeration in suspension were not observed through zeta potential (Figure S7) or DLS measurements (Figure S10).

In the present study, we have not investigated the toxicity of isolated AgNPs. However, previous reports have shown an improved antimicrobial property for hybrid CNC/Ag than pristine AgNPs.[75,76] Results obtained from plate count assays indicate an enhanced antibacterial activity for polydopamine-(PD)−CNC−Ag compared to pristine AgNPs.[76] For instance, PD−CNC−Ag presented a MIC of 8 μg/mL against *B. subtilis*, whereas pristine AgNPs showed a MIC of 32 μg/mL to the same bacteria.[76] In addition, cellulose nanowhiskers modified with AgNPs have shown a much lower MIC against *E. coli* than commercial AgNPs.[75] This improved toxicity for CNC−Ag is
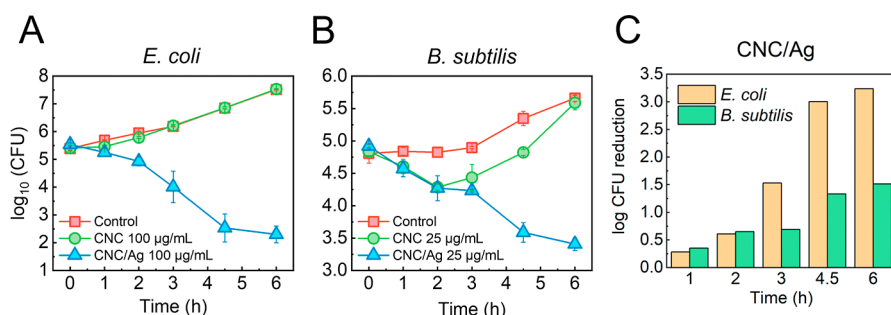
Figure 5. Time-dependent inactivation of (A) *E. coli* and (B) *B. subtilis* cells under exposure to CNC or CNC/Ag. The number of viable cells was quantified using the plate counting method and the value is expressed as the logarithm of colony-forming units (CFU). Error bars represent the standard deviation for three replicates ($n = 3$). (C) Number of log CFU reduction after exposure of *E. coli* and *B. subtilis* cells to CNC/Ag. The values for each bacteria strain were calculated by subtracting the value for each time point from its initial value (0 h).
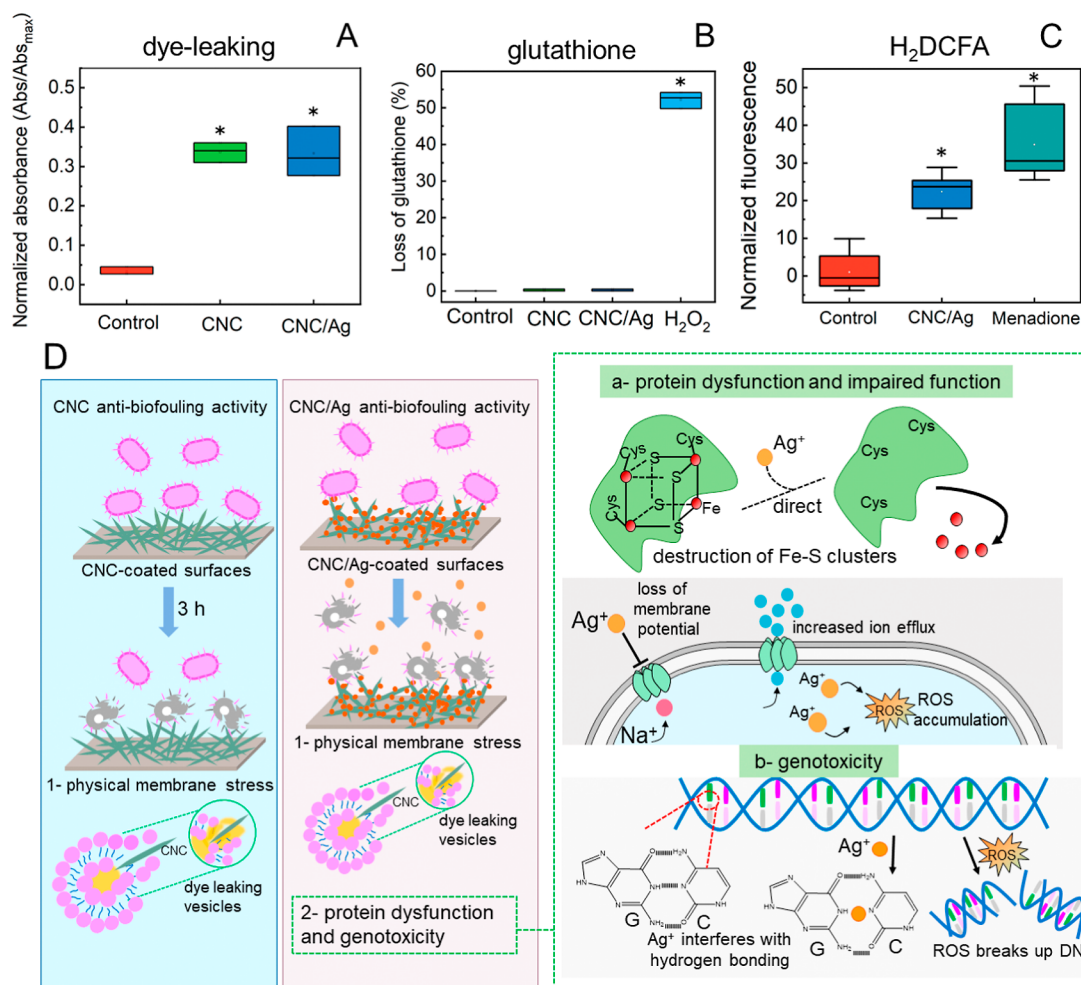
Figure 6. (A) Relative absorbance at 500 nm of acridine orange-containing vesicles after interacting with CNCs and CNC/Ag at 200 μg/mL and DI water (control). Absorbance values were normalized by the results obtained by SLS (0.1 g/mL) treatment. (B) Oxidation of GHS by CNCs and CNC/Ag after 3 h of contact. GHS solution (0.4 mM) was exposed to each nanomaterial dispersion (100 μg/mL) at room temperature in abiotic conditions. H_2O_2 was used as a positive control due to its oxidative properties. Loss of GHS is presented as a relative percentage to a control sample (DI water). Asterisks indicate a statistical difference from the control ($\alpha = 0.05$). (C) H_2DCFDA oxidative assay quantifying the generation of intracellular ROS by the bacteria cells exposed to CNC/Ag (100 μg/mL) and menadione (100 μM). Values were normalized based on the control samples (peptone water 0.1%). (D) Illustration demonstrating the mechanism by which CNC and CNC/Ag-coated surfaces inactivate attached bacteria cells. CNC-coated surfaces inactivate bacteria solely by membrane-stress-mediated mechanisms. CNC/Ag-coated surfaces use a dual mechanism of inactivation based on the membrane perforation by CNC and silver's ability to damage the cell membrane and the DNA. Similar illustrations demonstrating the antimicrobial mechanisms of action for silver can be found elsewhere.[78]

attributed to the anchoring of AgNPs on the CNC surface, which prevent losses in antimicrobial properties due to particle agglomeration.[75,76]

Antimicrobial Activity of CNCs and CNC/Ag to Planktonic Cells is Time-Dependent. Experiments were conducted with *E. coli* and *B. subtilis* to investigate the bacterial

growth kinetics under incubation with CNCs and CNC/Ag. Such assays are essential for assessing the interaction between the antimicrobial agent and the microbial strains and analyzing the time dependency of the antibacterial effect.[39] Each model bacteria was incubated with CNC/Ag at its respective MIC. Pristine CNC and CNC/Ag at their MIC concentrations (100 μg/mL for *E. coli* and 25 μg/mL for *B. subtilis*) were incubated with the bacteria cells for 6 h. Aliquots were collected along six-time points to determine the number of viable cells through plate counting (Figure 5).[39,40]

E. coli exposed to pristine CNCs presented similar growth trends to the control suspension (without a nanomaterial), suggesting that CNCs were not toxic to the bacteria under the tested conditions (Figure 5A). On the other hand, a significant 1.5 log CFU reduction occurred after *E. coli* cells were incubated with CNC/Ag, indicating a bactericidal effect against *E. coli*. We also observed a similar decrease in the number of viable *B. subtilis* cells after their exposure to CNCs and CNC/Ag within the first 2 h of incubation (Figure 5B). However, after 2 h, the *B. subtilis* cells incubated with CNCs grew almost exponentially, achieving similar numbers to the control after the incubation period is over. In contrast, the viability of *B. subtilis* cells decreases systematically overtime after contacting CNC/Ag. A 1.5 log CFU reduction, which corresponds to ~90% decrease in the number of viable cells, was detected for *B. subtilis* cells exposed to CNC/Ag, demonstrating the bactericidal effect promoted by the hybrid material.

Figure 5C shows the log CFU reduction for *E. coli* and *B. subtilis* after exposure to CNC/Ag throughout the time-kill assay. A compelling 1.5 log CFU decrease is observed for *E. coli* after 3 h exposure to CNC/Ag. In addition, the log CFU reduction increases as the exposure time between the cells and the hybrid material increases. *B. subtilis* cells reveal a similar log CFU reduction trend. However, we note a more drastic log CFU reduction for *B. subtilis* than *E. coli* cells. For example, after 6 h interaction with CNC/Ag, *E. coli* cells show a 3.0 log CFU reduction, unlike *B. subtilis*, which displays a significantly lower log CFU reduction of ~1.0. This result indicates that CNC/Ag inactivates *E. coli* quicker than *B. subtilis* cells at their respective MICs. Intrinsic differences in the cell wall composition and structure may explain the differences in antimicrobial properties between *E. coli* and *B. subtilis*. A thicker and more rigid layer of negatively charged peptidoglycans could hamper the diffusion of silver ions across the cell wall,[77] resulting in lower susceptibility to the effects of silver for Gram-positive *B. subtilis* than the Gram-negative *E. coli*. Although several studies have tried to address the antibacterial activity of CNC/Ag-based materials,[66,75,76] there is still a lack of fundamental understanding about the kinetics involving the interaction between bacteria and the CNC/Ag. At our account, this is the first systematic study demonstrating MIC, MBC, and time-dependent toxicity for CNC/Ag using Gram-positive and Gram-negative bacteria models.

Mechanisms of Action behind the Toxicity of CNC/Ag to Bacteria Cells. We used dye-containing phospholipidic vesicles mimicking the cell membrane to evaluate the CNC/Ag's ability to inactivate bacteria via physical-mediated membrane stress mechanisms (Figure 6). The release of encapsulated dye (e.g., acridine orange) upon contact of the CNC with the lipid vesicles strongly indicates that the nanomaterials can pierce the cell membrane and disturb the physical integrity of the phospholipid bilayer. The piercing holes affect the mechanisms of nutrient exchange with the environment, cause loss of intracellular content, and facilitate the penetration of Ag$^+$ ions within the cell upon exposure to CNC/Ag.

Figure 6A shows a relative increase in absorbance intensities due to dye leakage promoted by the interaction of CNC and CNC/Ag with the phospholipidic vesicles. These relative absorbance intensities were calculated by dividing the absorbance of each treatment by the maximum absorbance value obtained after disrupting the vesicles with a surfactant solution (SLS, 0.1 g/mL). The results of the control samples (lipid vesicles in DI water) show very low relative absorbance values after 3 h of the experiment, indicating a negligible dye efflux through vesicles over this period. Conversely, higher absorbance intensities for vesicles treated with CNCs and CNC/Ag indicate significant dye leakage and damage to the structure of the phospholipidic vesicles (Figure 6A). Similar relative absorbance values were obtained for both nanomaterials: 0.33 ± 0.02 for CNC and 0.33 ± 0.06 for CNC/Ag. These results suggest that CNCs and CNC/Ag have equivalent abilities to destabilize the lipid bilayer of cell membranes. This result is expected since both materials share the same needle-like morphology (Figures S3 and 2B).

We presume that the crystalline, rigid needle-like structure of CNCs and CNC/Ag is responsible for the contact-mediated damage promoted by these nanomaterials. Based on the results in Figure 6A, AgNPs attached on CNC seem to play no role in the physical-mediated cell membrane stress mechanism induced by CNCs. This observation leads us to assume that if the AgNPs on CNC/Ag interact with the membrane constituents, these interactions do not lead to significant cell membrane permeability changes under the tested conditions. Although CNC/Ag did not compromise membrane permeability, AgNPs could still impair membrane functionality by binding to transport proteins, affecting the cell uptake and efflux of essential ions.[78] In addition, these protein–Ag-based interactions can lead to membrane dysfunction, electron transport disruption, and enzyme activity loss. Metal intake can also explain the improved toxicity of CNC/Ag compared to pristine CNCs. While CNCs pierce the membrane, Ag$^+$ ions can enter the cell and promptly interact and damage the DNA, disrupting metabolic processes needed for the cell survival,[78] as illustrated in Figure 6D.

The GHS assay evaluated the CNC and CNC/Ag's ability to induce oxidation.[41] Generation of ROS, either by indirect or direct oxidation, is a toxicity mechanism commonly triggered by nanomaterials.[63,79] In this sense, a GHS oxidation assay was performed to investigate the oxidative properties of CNCs and CNC/Ag. Results have shown negligible increases in GHS oxidation for CNCs and CNC/Ag (0.16 and 0.32%, respectively) compared to the control group (Figure 6B). On the other hand, under the presence of a robust oxidative compound such as H$_2$O$_2$ (10 mM), GHS oxidation has achieved 52% after 3 h of interaction. These findings are in agreement with a previous study that demonstrates negligible GHS oxidation promoted by CNCs.[22]

We also investigated the presence of ROS inside the cells through the H$_2$DCFDA (2′,7′-dichlorodihydrofluorescein diacetate) assay using *E. coli* as the model organism. H$_2$DCFDA is permeable to the cell membrane of bacteria cells. Under the presence of ROS in the cell cytoplasm, H$_2$DCFDA transforms into DCF, a highly fluorescent compound that absorbs and emits light at 493/520 nm, respectively. The magnitude of the fluorescent signal generated by DCF can be correlated to the ROS level in the bacteria cells. Results for this assay are shown in

Figure 6C. A significant increase in the fluorescence signal at 520 nm was observed for *E. coli* exposed to CNC/Ag (100 μg/mL). CNC/Ag samples have averaged fluorescence values 22 times higher than the negative control. For example, the fluorescence signal for *E. coli* cells exposed to CNC/Ag exceeded 34 times the control. These results indicate that CNC/Ag can induce the accumulation of ROS inside the cells, corroborating with previous studies reporting oxidative stress mechanisms for Ag-containing materials.[63] A previous study of ours shows that CNC alone are unable to promote oxidation of H$_2$DCFDA into DCF.[22]

Although the GHS assay shows that CNC/Ag is not promoting direct oxidation via ROS production, the H$_2$DCFDA assay confirms an accumulation of ROS inside the cells exposed to the nanomaterial. Therefore, CNC/Ag may not induce or accelerate ROS production, but it leads to indirect oxidative stress due to accumulation of ROS within the cells. ROS accumulation in the cells can cause several damages to organelles, proteins, and the DNA, as illustrated in Figure 6D. In addition to indirect oxidation mechanisms, it is worth mentioning that Ag$^+$ ions could still be binding to specific functional groups of proteins and enzymes, causing localized oxidation processes (ROS-independent) in these essential biomolecules.[63,80] Therefore, silver could be participating in redox reactions by binding selectively to atoms of donor ligands, such as oxygen, nitrogen, and sulfur. Replacing the correct metal cofactor by Ag$^+$ ions can interfere with protein folding and function.[78] Abundant presence of Ag$^+$ ions can prevent proteins from acquiring the correct metal cofactor, which will lead to a metabolic collapse and cell death (Figure 6D).

CONCLUSIONS

This study demonstrates the deposition of AgNPs on the surface of CNCs for improved anti-biofouling and antimicrobial properties. The anchoring of AgNPs on CNCs (CNC/Ag) was performed in situ using sodium borohydride. Anchored AgNPs showed an average diameter of 10.3 nm and were well-distributed on the CNC surface. Our findings show that functionalization with AgNPs significantly improve the anti-biofouling property of CNCs. For example, the ability of CNC-coated surfaces to inactivate bacteria cells (both Gram-negative and Gram-positive) increased from 33 to 65% to almost 100% after CNC modification with AgNPs. In this sense, CNC/Ag shows excellent potential as antimicrobial coatings for anti-biofouling applications in medicine and engineering. CNC/Ag also showed high toxicity against *E. coli* and *B. subtilis* planktonic cells, confirming that the material can inactivate bacteria in suspension before surface attachment. Minimum inhibitory concentrations were 25 and 100 μg/mL against *B. subtilis* and *E. coli*, respectively. Time-kill assays showed that CNC/Ag inactivate planktonic Gram-negative *E. coli* cells faster than Gram-positive *B. subtilis*, revealing that the antibacterial kinetics of CNC/Ag is affected by the structure and composition of the bacteria cell wall. Very low toxicity was observed for pristine CNCs against planktonic cells of both microorganisms. Dye-leaking assays revealed that CNCs and CNC/Ag promote disruption of the lipid bilayer and can inactivate bacteria cells under physical-mediated mechanisms. The GHS suggested that neither CNCs nor CNC/Ag was able to induce oxidative stress through direct production of ROS. However, accumulation of ROS inside the cell was found for bacteria cells exposed to CNC/Ag after 3 h exposure. This indicates that CNC/Ag may not oxidize the cell via direct ROS generation, but they somehow

interfere with the cellular antioxidant mechanisms used to maintain ROS at low levels within the cytoplasm. In this way, we propose that the mechanism of action for CNC/Ag combines an attacking–attacking strategy that includes the physical membrane stress promoted by the narrow CNC and the disruption of vital metabolic processes caused by the anchored AgNPs.

ASSOCIATED CONTENT

ⓈI Supporting Information

The Supporting Information is available free of charge at https://pubs.acs.org/doi/10.1021/acsabm.1c00929.

XRD, thermogravimetric analysis, zeta potential measurements, DLS analysis, UV–vis spectroscopy stability analysis. Biofilm characterization through confocal microscopy, XRD profiles of CNC and CNC/Ag, thermogravimetric analysis of CNC and CNC/Ag, microplate wells with CNC and *Bacillus* sp. suspensions, XPS survey spectra for CNC and CNC/Ag hybrid material, ATR-FTIR spectra of CNC and CNC/Ag, Ag$^+$ releasing profile of CNC/Ag in water as a function of the time, CLSM three-dimensional representative images, zeta potential distribution for CNC and CNC/Ag at pH 5, hydrodynamic diameter of CNC/Ag (300 μg/mL) dispersed in LB broth and DI water over 6 h of DLS measurements, UV–vis spectra kinetics of CNC/Ag dispersed in LB broth at 100 μg/mL (PDF)

AUTHOR INFORMATION

Corresponding Author

Andreia F. Faria — *Engineering School of Sustainable Infrastructure & Environment, Department of Environmental Engineering Sciences, University of Florida, Gainesville, Florida 32611-6540, United States;* Ⓞorcid.org/0000-0001-7473-040X; Phone: 352-392-7104; Email: andreia.faria@essie.ufl.edu

Authors

Victor T. Noronha — *Engineering School of Sustainable Infrastructure & Environment, Department of Environmental Engineering Sciences, University of Florida, Gainesville, Florida 32611-6540, United States; Solid-Biological Interfaces Group, Department of Physics, Federal University of Ceará—UFC, Fortaleza, Ceará 60455-900, Brazil;* ⓄNorcid.org/0000-0002-9643-5812

Jennifer C. Jackson — *Engineering School of Sustainable Infrastructure & Environment, Department of Environmental Engineering Sciences, University of Florida, Gainesville, Florida 32611-6540, United States*

Camilla H. M. Camargos — *Physical Chemistry Department, Institute of Chemistry, University of Campinas—UNICAMP, Campinas, São Paulo 13083-970, Brazil;* Ⓞorcid.org/0000-0002-5240-036X

Amauri J. Paula — *Solid-Biological Interfaces Group, Department of Physics, Federal University of Ceará—UFC, Fortaleza, Ceará 60455-900, Brazil; Ilum School of Science, Centro Nacional de Pesquisa em Energia e Materiais—CNPEM, Campinas, São Paulo 13087-548, Brazil*

Camila A. Rezende — *Physical Chemistry Department, Institute of Chemistry, University of Campinas—UNICAMP, Campinas, São Paulo 13083-970, Brazil;* Ⓞorcid.org/0000-0002-2072-1361

Complete contact information is available at:

https://pubs.acs.org/10.1021/acsabm.1c00929

■ REFERENCES

(1) Procópio, L. The Role of Biofilms in the Corrosion of Steel in Marine Environments. *World J. Microbiol. Biotechnol.* **2019**, *35*, 73.

(2) Flemming, H.-C.; Schaule, G.; Griebe, T.; Schmitt, J.; Tamachkiarowa, A. Biofouling—the Achilles Heel of Membrane Processes. *Desalination* **1997**, *113*, 215−225.

(3) Bar-Zeev, E.; Perreault, F.; Straub, A. P.; Elimelech, M. Impaired Performance of Pressure-Retarded Osmosis Due to Irreversible Biofouling. *Environ. Sci. Technol.* **2015**, *49*, 13050−13058.

(4) Jiang, S.; Li, Y.; Ladewig, B. P. A Review of Reverse Osmosis Membrane Fouling and Control Strategies. *Sci. Total Environ.* **2017**, *595*, 567−583.

(5) Hori, K.; Matsumoto, S. Bacterial Adhesion: From Mechanism to Control. *Biochem. Eng. J.* **2010**, *48*, 424−434.

(6) Kumar, C. G.; Anand, S. K. Significance of Microbial Biofilms in Food Industry: A Review. *Int. J. Food Microbiol.* **1998**, *42*, 9−27.

(7) Davies, D. Understanding Biofilm Resistance to Antibacterial Agents. *Nat. Rev. Drug Discovery* **2003**, *2*, 114−122.

(8) Khatoon, Z.; McTiernan, C. D.; Suuronen, E. J.; Mah, T.-F.; Alarcon, E. I. Bacterial Biofilm Formation on Implantable Devices and Approaches to Its Treatment and Prevention. *Heliyon* **2018**, *4*, No. e01067.

(9) Pinto, R. M.; Lopes-De-Campos, D.; Martins, M. C. L.; Van Dijck, P.; Nunes, C.; Reis, S. Impact of Nanosystems in Staphylococcus Aureus Biofilms Treatment. *FEMS Microbiol. Rev.* **2019**, *43*, 622−641.

(10) Mebert, A. M.; Villanueva, M. E.; Catalano, P. N.; Copello, G. J.; Bellino, M. G.; Alvarez, G. S.; Desimone, M. F. Surface Chemistry of Nanobiomaterials with Antimicrobial Activity. *Surface Chemistry of Nanobiomaterials*; Elsevier, 2016; pp 135−162. **In Memoriam of Professor Dr. Luis Diaz.

(11) Garrett, T. R.; Bhakoo, M.; Zhang, Z. Bacterial Adhesion and Biofilms on Surfaces. *Prog. Nat. Sci.* **2008**, *18*, 1049−1056.

(12) Perreault, F.; De Faria, A. F.; Nejati, S.; Elimelech, M. Antimicrobial Properties of Graphene Oxide Nanosheets: Why Size Matters. *ACS Nano* **2015**, *9*, 7226−7236.

(13) Rodrigues, D. F.; Jaisi, D. P.; Elimelech, M. Toxicity of Functionalized Single-Walled Carbon Nanotubes on Soil Microbial Communities: Implications for Nutrient Cycling in Soil. *Environ. Sci. Technol.* **2013**, *47*, 625−633.

(14) Wei, G.; Dong, J.; Bai, J.; Zhao, Y.; Li, Y. Structurally Stable, Antifouling, and Easily Renewable Reduced Graphene Oxide Membrane with a Carbon Nanotube Protective Layer. *Environ. Sci. Technol.* **2019**, *53*, 11896−11903.

(15) Perreault, F.; Fonseca de Faria, A.; Elimelech, M. Environmental Applications of Graphene-Based Nanomaterials. *Chem. Soc. Rev.* **2015**, *44*, 5861−5896.

(16) de Faria, A. F.; Martinez, D. S. T.; Meira, S. M. M.; de Moraes, A. C. M.; Filho, A. G. S.; Alves, O. L.; Alves, O. L. Anti-Adhesion and Antibacterial Activity of Silver Nanoparticles Supported on Graphene Oxide Sheets. *Colloids Surf., B* **2014**, *113*, 115−124.

(17) De Faria, A. F.; Perreault, F.; Shaulsky, E.; Arias Chavez, L. H.; Elimelech, M. Antimicrobial Electrospun Biopolymer Nanofiber Mats Functionalized with Graphene Oxide−Silver Nanocomposites. *ACS Appl. Mater. Interfaces* **2015**, *7*, 12751−12759.

(18) Moraes, A. C. M. d.; Araujo Lima, B.; Fonseca de Faria, A.; Brocchi, M.; Luiz Alves, O. Graphene Oxide-Silver Nanocomposite as a Promising Biocidal Agent against Methicillin-Resistant Staphylococcus Aureus. *Int. J. Nanomed.* **2015**, *10*, 6847.

(19) Faria, A. F.; Liu, C.; Xie, M.; Perreault, F.; Nghiem, L. D.; Ma, J.; Elimelech, M. Thin-Film Composite Forward Osmosis Membranes Functionalized with Graphene Oxide−Silver Nanocomposites for Biofouling Control. *J. Membr. Sci.* **2017**, *525*, 146−156.

(20) Cheng, G.; Zhang, Z.; Chen, S.; Bryers, J. D.; Jiang, S. Inhibition of Bacterial Adhesion and Biofilm Formation on Zwitterionic Surfaces. *Biomaterials* **2007**, *28*, 4192−4199.

(21) Liu, C.; Lee, J.; Ma, J.; Elimelech, M. Antifouling Thin-Film Composite Membranes by Controlled Architecture of Zwitterionic Polymer Brush Layer. *Environ. Sci. Technol.* **2017**, *51*, 2161−2169.

(22) Noronha, V. T.; Camargos, C. H. M.; Jackson, J. C.; Souza Filho, A. G.; Paula, A. J.; Rezende, C. A.; Faria, A. F. Physical Membrane-Stress-Mediated Antimicrobial Properties of Cellulose Nanocrystals. *ACS Sustainable Chem. Eng.* **2021**, *9*, 3203−3212.

(23) Du, L.; Arnholt, K.; Ripp, S.; Sayler, G.; Wang, S.; Liang, C.; Wang, J.; Zhuang, J. Biological Toxicity of Cellulose Nanocrystals (CNCs) against the LuxCDABE-Based Bioluminescent Bioreporter Escherichia Coli 652T7. *Ecotoxicology* **2015**, *24*, 2049−2053.

(24) Mahmoud, K. A.; Mena, J. A.; Male, K. B.; Hrapovic, S.; Kamen, A.; Luong, J. H. T. Effect of Surface Charge on the Cellular Uptake and Cytotoxicity of Fluorescent Labeled Cellulose Nanocrystals. *ACS Appl. Mater. Interfaces* **2010**, *2*, 2924−2932.

(25) Mou, K.; Li, J.; Wang, Y.; Cha, R.; Jiang, X. 2,3-Dialdehyde Nanofibrillated Cellulose as a Potential Material for the Treatment of MRSA Infection. *J. Mater. Chem. B* **2017**, *5*, 7876−7884.

(26) Lv, J.; Zhang, X.; Yu, N.; Su, S.; Zhu, J.; Deng, L.; Liu, Z. One-Pot Synthesis of CNC-Ag@AgCl with Antifouling and Antibacterial Properties. *Cellulose* **2019**, *26*, 7837−7846.

(27) Liu, K.; Liang, H.; Nasrallah, J.; Chen, L.; Huang, L.; Ni, Y. Preparation of the CNC/Ag/Beeswax Composites for Enhancing Antibacterial and Water Resistance Properties of Paper. *Carbohydr. Polym.* **2016**, *142*, 183−188.

(28) He, J.; Kunitake, T.; Nakao, A. Facile In Situ Synthesis of Noble Metal Nanoparticles in Porous Cellulose Fibers. *Chem. Mater.* **2003**, *15*, 4401−4406.

(29) Caschera, D.; Toro, R. G.; Federici, F.; Montanari, R.; de Caro, T.; Al-Shemy, M. T.; Adel, A. M. Green Approach for the Fabrication of Silver-Oxidized Cellulose Nanocomposite with Antibacterial Properties. *Cellulose* **2020**, *27*, 8059−8073.

(30) Ye, G.; Lee, J.; Perreault, F.; Elimelech, M. Controlled Architecture of Dual-Functional Block Copolymer Brushes on Thin-Film Composite Membranes for Integrated "Defending" and "Attacking" Strategies against Biofouling. *ACS Appl. Mater. Interfaces* **2015**, *7*, 23069−23079.

(31) Dai, G.; Ai, X.; Mei, L.; Ma, C.; Zhang, G. Kill−Resist−Renew Trinity: Hyperbranched Polymer with Self-Regenerating Attack and Defense for Antifouling Coatings. *ACS Appl. Mater. Interfaces* **2021**, *13*, 13735−13743.

(32) Liu, C.; Faria, A. F.; Jackson, J.; He, Q.; Ma, J. Enhancing the Anti-Fouling and Fouling Removal Properties of Thin-Film Composite Membranes through an Intercalated Functionalization Method. *Environ. Sci.: Water Res. Technol.* **2021**, *7*, 1336−1347.

(33) Bai, L.; Liu, Y.; Ding, A.; Ren, N.; Li, G.; Liang, H. Fabrication and Characterization of Thin-Film Composite (TFC) Nanofiltration Membranes Incorporated with Cellulose Nanocrystals (CNCs) for Enhanced Desalination Performance and Dye Removal. *Chem. Eng. J.* **2019**, *358*, 1519−1528.

(34) Xu, C.; Chen, W.; Gao, H.; Xie, X.; Chen, Y. Cellulose Nanocrystal/Silver (CNC/Ag) Thin-Film Nanocomposite Nanofiltration Membranes with Multifunctional Properties. *Environ. Sci.: Nano* **2020**, *7*, 803−816.

(35) Camargos, C. H. M.; Rezende, C. A. Structure−Property Relationships of Cellulose Nanocrystals and Nanofibrils: Implications for the Design and Performance of Nanocomposites and All-Nanocellulose Systems. *ACS Appl. Nano Mater.* **2021**, *4*, 10505−10518.

(36) Liu, H.; Wang, D.; Song, Z.; Shang, S. Preparation of Silver Nanoparticles on Cellulose Nanocrystals and the Application in Electrochemical Detection of DNA Hybridization. *Cellulose* **2011**, *18*, 67−74.

(37) Xu, X.; Yang, Y.-Q.; Xing, Y.-Y.; Yang, J.-F.; Wang, S.-F. Properties of Novel Polyvinyl Alcohol/Cellulose Nanocrystals/Silver Nanoparticles Blend Membranes. *Carbohydr. Polym.* **2013**, *98*, 1573−1577.

(38) Jackson, J. C.; Camargos, C. H. M.; Noronha, V. T.; Paula, A. J.; Rezende, C. A.; Faria, A. F. Sustainable Cellulose Nanocrystals for Improved Antimicrobial Properties of Thin Film Composite Membranes. *ACS Sustainable Chem. Eng.* **2021**, *9*, 6534−6540.

(39) Balouiri, M.; Sadiki, M.; Ibnsouda, S. K. Methods for in Vitro Evaluating Antimicrobial Activity: A Review. *J. Pharm. Anal.* **2016**, *6*, 71−79.

(40) Konaté, K.; Mavoungou, J.; Lepengué, A.; Aworet-Samseny, R. R.; Hilou, A.; Souza, A.; Dicko, M. H.; M'Batchi, B. Antibacterial Activity against β- Lactamase Producing Methicillin and Ampicillin-Resistants Staphylococcus Aureus: Fractional Inhibitory Concentration Index (FICI) Determination. *Ann. Clin. Microbiol. Antimicrob.* **2012**, *11*, 18.

(41) Hellack, B.; Nickel, C.; Albrecht, C.; Kuhlbusch, T. A. J.; Boland, S.; Baeza-Squiban, A.; Wohlleben, W.; Schins, R. P. F. Analytical Methods to Assess the Oxidative Potential of Nanoparticles: A Review. *Environ. Sci.: Nano* **2017**, *4*, 1920−1934.

(42) Fahey, R. C.; Brown, W. C.; Adams, W. B.; Worsham, M. B. Occurrence of Glutathione in Bacteria. *J. Bacteriol.* **1978**, *133*, 1126−1129.

(43) Kurutas, E. B. The Importance of Antioxidants Which Play the Role in Cellular Response against Oxidative/Nitrosative Stress: Current State. *Nutr. J.* **2015**, *15*, 71.

(44) Barrios, A. C.; Wang, Y.; Gilbertson, L. M.; Perreault, F. Structure−Property−Toxicity Relationships of Graphene Oxide: Role of Surface Chemistry on the Mechanisms of Interaction with Bacteria. *Environ. Sci. Technol.* **2019**, *53*, 14679−14687.

(45) Criddle, D. N.; Gillies, S.; Baumgartner-Wilson, H. K.; Jaffar, M.; Chinje, E. C.; Passmore, S.; Chvanov, M.; Barrow, S.; Gerasimenko, O. V.; Tepikin, A. V.; Sutton, R.; Petersen, O. H. Menadione-Induced Reactive Oxygen Species Generation via Redox Cycling Promotes Apoptosis of Murine Pancreatic Acinar Cells. *J. Biol. Chem.* **2006**, *281*, 40485−40492.

(46) Zucker, I.; Hashmi, S. M.; Yang, J.; He, Y.; Pfefferle, L. D.; Elimelech, M. Shape-Dependent Interactions of Manganese Oxide Nanomaterials with Lipid Bilayer Vesicles. *Langmuir* **2019**, *35*, 13958−13966.

(47) Zucker, I.; Werber, J. R.; Fishman, Z. S.; Hashmi, S. M.; Gabinet, U. R.; Lu, X.; Osuji, C. O.; Pfefferle, L. D.; Elimelech, M. Loss of Phospholipid Membrane Integrity Induced by Two-Dimensional Nanomaterials. *Environ. Sci. Technol. Lett.* **2017**, *4*, 404−409.

(48) Lu, X.; Feng, X.; Werber, J. R.; Chu, C.; Zucker, I.; Kim, J.-H.; Osuji, C. O.; Elimelech, M. Enhanced Antibacterial Activity through the Controlled Alignment of Graphene Oxide Nanosheets. *Proc. Natl. Acad. Sci.* **2017**, *114*, E9793−E9801.

(49) Ifuku, S.; Tsuji, M.; Morimoto, M.; Saimoto, H.; Yano, H. Synthesis of Silver Nanoparticles Templated by TEMPO-Mediated Oxidized Bacterial Cellulose Nanofibers. *Biomacromolecules* **2009**, *10*, 2714−2717.

(50) Hoeng, F.; Denneulin, A.; Neuman, C.; Bras, J. Charge Density Modification of Carboxylated Cellulose Nanocrystals for Stable Silver Nanoparticles Suspension Preparation. *J. Nanopart. Res.* **2015**, *17*, 1−14.

(51) Smitha, S. L.; Nissamudeen, K. M.; Philip, D.; Gopchandran, K. G. Studies on Surface Plasmon Resonance and Photoluminescence of Silver Nanoparticles. *Spectrochim. Acta, Part A* **2008**, *71*, 186−190.

(52) Park, S.; Baker, J. O.; Himmel, M. E.; Parilla, P. A.; Johnson, D. K. Cellulose Crystallinity Index: Measurement Techniques and Their Impact on Interpreting Cellulase Performance. *Biotechnol. Biofuels* **2010**, *3*, 10.

(53) Alharthi, F. A.; Alghamdi, A. A.; Al-Zaqri, N.; Alanazi, H. S.; Alsyahi, A. A.; Marghany, A. E.; Ahmad, N. Facile One-Pot Green Synthesis of Ag−ZnO Nanocomposites Using Potato Peeland Their Ag Concentration Dependent Photocatalytic Properties. *Sci. Rep.* **2020**, *10*, 1−14.

(54) Liu, J.; Guo, Q.; Mao, S.; Chen, Z.; Zhang, X.; Yang, Y.; Zhang, X. Templated Synthesis of a 1D Ag Nanohybrid in the Solid State and Its Organized Network for Strain-Sensing Applications. *J. Mater. Chem. C* **2018**, *6*, 10730−10738.

(55) Errokh, A.; Magnin, A.; Putaux, J.-L.; Boufi, S. Hybrid Nanocellulose Decorated with Silver Nanoparticles as Reinforcing Filler with Antibacterial Properties. *Mater. Sci. Eng., C* **2019**, *105*, 110044.

(56) Fan, L.; Zhang, H.; Gao, M.; Zhang, M.; Liu, P.; Liu, X. Cellulose Nanocrystals/Silver Nanoparticles: In-Situ Preparation and Application in PVA Films. *Holzforschung* **2019**, *74*, 523−528.

(57) Ma, Z.; Liu, J.; Shen, G.; Zheng, X.; Pei, Y.; Tang, K. In-Situ Synthesis and Immobilization of Silver Nanoparticles on Microfibrillated Cellulose for Long-Term Antibacterial Applications. *Cellulose* **2021**, *28*, 6287−6303.

(58) Zhu, J.; Tang, T.; Hu, C.-Y.; Xiang, W.-C.; Chen, Z.-Q.; Luo, L.; Yang, H.-S.; Liu, H.-P. Cellulose Nanocrystal Assisted Trace Silver Nitrate to Synthesize Green Silver Nanocomposites with Antibacterial Activity. *RSC Adv.* **2021**, *11*, 3808−3815.

(59) Goswami, M.; Baruah, D.; Das, A. M. Green Synthesis of Silver Nanoparticles Supported on Cellulose and Their Catalytic Application in the Scavenging of Organic Dyes. *New J. Chem.* **2018**, *42*, 10868−10878.

(60) Kumar, R.; Münstedt, H. Silver Ion Release from Antimicrobial Polyamide/Silver Composites. *Biomaterials* **2005**, *26*, 2081−2088.

(61) Faria, A. F.; Perreault, F.; Elimelech, M. Elucidating the Role of Oxidative Debris in the Antimicrobial Properties of Graphene Oxide. *ACS Appl. Nano Mater.* **2018**, *1*, 1164−1174.

(62) Tyagi, P.; Mathew, R.; Opperman, C.; Jameel, H.; Gonzalez, R.; Lucia, L.; Hubbe, M.; Pal, L. High-Strength Antibacterial Chitosan−

Cellulose Nanocrystal Composite Tissue Paper. *Langmuir* **2019**, *35*, 104−112.

(63) Le Ouay, B.; Stellacci, F. Antibacterial Activity of Silver Nanoparticles: A Surface Science Insight. *Nano Today* **2015**, *10*, 339−354.

(64) Paula, A. J.; Hwang, G.; Koo, H. Dynamics of Bacterial Population Growth in Biofilms Resemble Spatial and Structural Aspects of Urbanization. *Nat. Commun.* **2020**, *11*, 1354.

(65) Riley, E. P.; Schwarz, C.; Derman, A. I.; Lopez-Garrido, J. Milestones in Bacillus Subtilis Sporulation Research. *Microb. Cell* **2021**, *8*, 1−16.

(66) Spagnol, C.; Fragal, E. H.; Pereira, A. G. B.; Nakamura, C. V.; Muniz, E. C.; Follmann, H. D. M.; Silva, R.; Rubira, A. F. Cellulose Nanowhiskers Decorated with Silver Nanoparticles as an Additive to Antibacterial Polymers Membranes Fabricated by Electrospinning. *J. Colloid Interface Sci.* **2018**, *531*, 705−715.

(67) Zirehpour, A.; Rahimpour, A.; Arabi Shamsabadi, A.; Sharifian, G. M.; Soroush, M. Mitigation of Thin-Film Composite Membrane Biofouling via Immobilizing Nano-Sized Biocidal Reservoirs in the Membrane Active Layer. *Environ. Sci. Technol.* **2017**, *51*, 5511−5522.

(68) Firouzjaei, M. D.; Shamsabadi, A. A.; Sharifian, G. M.; Rahimpour, A.; Soroush, M. A Novel Nanocomposite with Superior Antibacterial Activity: A Silver-Based Metal Organic Framework Embellished with Graphene Oxide. *Adv. Mater. Interfaces* **2018**, *5*, 1701365.

(69) Firouzjaei, M. D.; Shamsabadi, A. A.; Aktij, S. A.; Seyedpour, S. F.; Sharifian, G. M.; Rahimpour, A.; Esfahani, M. R.; Ulbricht, M.; Soroush, M. Exploiting Synergetic Effects of Graphene Oxide and a Silver-Based Metal−Organic Framework To Enhance Antifouling and Anti-Biofouling Properties of Thin-Film Nanocomposite Membranes. *ACS Appl. Mater. Interfaces* **2018**, *10*, 42967−42978.

(70) de Faria, A. F.; de Moraes, A. C. M.; da Silva, D. S.; do Carmo Gonçalves, M.; Alves, O. L.; Alves, O. L. Cellulose Acetate Membrane Embedded with Graphene Oxide-Silver Nanocomposites and Its Ability to Suppress Microbial Proliferation. *Cellulose* **2017**, *24*, 781−796.

(71) Cao, T.; Elimelech, M. Colloidal Stability of Cellulose Nanocrystals in Aqueous Solutions Containing Monovalent, Divalent, and Trivalent Inorganic Salts. *J. Colloid Interface Sci.* **2021**, *584*, 456−463.

(72) Jakubek, Z. J.; Chen, M.; Couillard, M.; Leng, T.; Liu, L.; Zou, S.; Baxa, U.; Clogston, J. D.; Hamad, W. Y.; Johnston, L. J. Characterization Challenges for a Cellulose Nanocrystal Reference Material: Dispersion and Particle Size Distributions. *J. Nanopart. Res.* **2018**, *20*, 98.

(73) Tejamaya, M.; Römer, I.; Merrifield, R. C.; Lead, J. R. Stability of Citrate, PVP, and PEG Coated Silver Nanoparticles in Ecotoxicology Media. *Environ. Sci. Technol.* **2012**, *46*, 7011−7017.

(74) Argentiere, S.; Cella, C.; Cesaria, M.; Milani, P.; Lenardi, C. Silver Nanoparticles in Complex Biological Media: Assessment of Colloidal Stability and Protein Corona Formation. *J. Nanopart. Res.* **2016**, *18*, 1−13.

(75) Wang, S.; Sun, J.; Jia, Y.; Yang, L.; Wang, N.; Xianyu, Y.; Chen, W.; Li, X.; Cha, R.; Jiang, X. Nanocrystalline Cellulose-Assisted Generation of Silver Nanoparticles for Nonenzymatic Glucose Detection and Antibacterial Agent. *Biomacromolecules* **2016**, *17*, 2472−2478.

(76) Shi, Z.; Tang, J.; Chen, L.; Yan, C.; Tanvir, S.; Anderson, W. A.; Berry, R. M.; Tam, K. C. Enhanced Colloidal Stability and Antibacterial Performance of Silver Nanoparticles/Cellulose Nanocrystal Hybrids. *J. Mater. Chem. B* **2015**, *3*, 603−611.

(77) Dakal, T. C.; Kumar, A.; Majumdar, R. S.; Yadav, V. Mechanistic Basis of Antimicrobial Actions of Silver Nanoparticles. *Front. Microbiol.* **2016**, *7*, 1831.

(78) Lemire, J. A.; Harrison, J. J.; Turner, R. J. Antimicrobial Activity of Metals: Mechanisms, Molecular Targets and Applications. *Nat. Rev. Microbiol.* **2013**, *11*, 371−384.

(79) Sharifi, S.; Behzadi, S.; Laurent, S.; Laird Forrest, M.; Stroeve, P.; Mahmoudi, M. Toxicity of Nanomaterials. *Chem. Soc. Rev.* **2012**, *41*, 2323−2343.

(80) Qing, Y. a.; Cheng, L.; Li, R.; Liu, G.; Zhang, Y.; Tang, X.; Wang, J.; Liu, H.; Qin, Y. Potential Antibacterial Mechanism of Silver Nanoparticles and the Optimization of Orthopedic Implants by Advanced Modification Technologies. *Int. J. Nanomed.* **2018**, *13*, 3311−3327.

■ NOTE ADDED AFTER ASAP PUBLICATION

This article originally published with errors in the caption of Figure 2. The caption was corrected and reposted February 18, 2022.

▣ Recommended by ACS